Estimation of elastic modulus, fracture toughness and strength of 47.5B-derived bioactive glass-ceramics for bone scaffold applications: a nanoindentation study

Estimation of elastic modulus, fracture toughness and strength of 47.5B-derived bioactive glass-ceramics for bone scaffold applications: a nanoindentation study

Luca D'Andrea[a], Anna De Cet[a], Dario Gastaldi[a], Francesco Baino[b], Enrica Verné[b], Pasquale Vena[a,*]

[a]*Department of Chemistry, Materials and Chemical Engineering Giulio Natta, Laboratory of Biological Structure Mechanics (LaBS) - Politecnico di Milano, Piazza Leonardo da Vinci 32, 20133, Milano, Italy*

[b]*Institute of Materials Physics and Engineering, Department of Applied Science and Technology - Politecnico di Torino, 10129 Torino, Italy*

Abstract

The knowledge of the mechanical properties of glass-ceramic materials used in bone scaffolds is the key to the optimal design of tissue engineering devices. In this paper, the elastic properties and fracture toughness of silicate bioactive glass-ceramics based on the 47.5B parent composition were quantified for the first time through nanoindentation. Specifically, the effect of sintering temperature was investigated by testing samples sintered at six different temperatures.

The samples sintered at higher temperatures exhibited elastic modulus and fracture toughness higher than those of the lower temperature samples. Both properties are comparable with those shown by similar bioactive glasses available in literature, supporting the mechanical suitability of the materials for bone applications.

An estimation of tensile strength as a function of flaw size is also provided by means of fracture mechanics approaches.

Keywords: bioactive glass-ceramic, micromechanical characterization, nanoindentation, sintering temperature

1. Introduction

Bioactive glasses are promising biomaterials for Bone Tissue Engineering (BTE) scaffolds [1, 2], as they are biocompatible, osteoconductive and able to create a stable tissue/device interface [3, 4].

Load bearing applications of BTE scaffolds impose particular emphasis on mechanical

*Corresponding author

Email addresses: luca.dandrea@polimi.it (Luca D'Andrea), anna.decet@polimi.it (Anna De Cet), dario.gastaldi@polimi.it (Dario Gastaldi), francesco.baino@polito.it (Francesco Baino), enrica.verne@polito.it (Enrica Verné), pasquale.vena@polimi.it (Pasquale Vena)

properties, especially in devices requiring high porosity, that makes them prone to fracture. Bioglass® 45S5 and other silicate glasses have been used to manufacture scaffolds with low-to-adequate mechanical properties for bone repair [1, 5, 6] by means of the foam replication technique. However, different micro-defect distribution or different degrees of crystallinity, depending on sintering temperature, have effect on the elastic, strength and toughness properties of the solid constituent and of the entire scaffold. In [7] the sinter-crystallization of a highly-bioactive glass (47.5B composition) in the range of 600 to 850°C was studied to assess the relationship between the sintering temperature and the mechanical properties of the porous scaffolds produced thereof. The aim of this work is to assess the elastic and toughness properties of the solid phase in the bioactive glass-derived scaffolds developed in [7]. The study is performed on suitably produced bulk samples through pellet sintering, following the same procedure as in [7]; in particular the effect of temperature on the intrinsic mechanical properties of the materials was investigated, ruling out the substantial effect of macroscopic scaffold porosity on the material mechanical response.

2. Materials and Methods

2.1. Sample preparation and nanoindentation tests

An experimental bioactive glass composition ($47.5SiO_2-10Na_2O-10K_2O-10MgO-20CaO_2-2.5P_2O_5\,mol\%$), referred to as 47.5B, was used to produce the bulk samples, which were obtained through melt-quenching route followed by pelletization of glass powders (particle size $< 32\ \mu m$) and sintering for 3 h at 600, 650, 700, 750, 800 and 850°C [7].

Berkovich and spherical (tip radius 10 μm) nanoindentations were carried out on one sample for each selected sintering temperature after embedding in epoxy resin and mirror-polishing. Nanoindentation tests were performed on Nanotest Platform3 (MicroMaterials) at controlled temperature of 28°C.

The testing parameters are reported in table 1. Berkovich indentations at peak load of 10 mN, 50 mN, 100 mN and 200 mN were used to obtain elastic properties; indentations at 400 mN were used to assess the fracture toughness. Spherical indentations were used to confirm elastic properties (peak load 100 mN) and produce crack patterns to predict a maximum material tensile strength (peak load 400 mN).

Thermal drift corrections were assessed by holding a constant load at 10% of the maximum load during the unloading phase.

A matrix of 25 indentations was performed for each indenter and each maximum load.

The reduce modulus E^* and the hardness H were obtained from the unloading part of the Berkovich nanoindentation curves by means of the Oliver and Pharr procedure [8]. The indentation modulus M^* is obtained as:

$$\frac{1}{M^*} = \frac{1}{E^*} - \frac{1-\nu_i^2}{E_i} \tag{1}$$

in which ν_i and E_i are Poisson ratio and Young modulus of the indenter. The indentation modulus M^* is related to the material properties (E_s and ν_s) under the hypothesis of linear isotropy as:

$$M^* = \frac{E_s}{1-\nu_s^2} \tag{2}$$

2

Indenter	Peak Load [mN]	Loading Rate [mN/s]	Holding Time [s]	Unloading Rate [mN/s]
Berkovich	10	2.5	3	5
	50	2.5	3	5
	100	2.5	3	5
	200	2.5	3	5
	400	10	3	20
Spherical	100	2.5	3	5
	400	2.5	3	5

Table 1: Nanoindentation tests parameters.

The mechanical properties of the diamond tip Berkovich indenter and silicon carbide spherical indenters are: $E_{i,B} = 1171\,GPa$ and $\nu_{i,B} = 0.07$, $E_{i,S} = 511\,GPa$ and $\nu_{i,S} = 0.17$, respectively.

2.2. Bulk glass-ceramic fracture toughness

The crack patterns induced during indentation were observed through Confocal laser imaging (Olympus LEXT OLS4100 3D Measuring Microscope). The 100X magnification was used to obtain the highest image resolution. The laser intensity and height images were overlapped to enhance crack visibility.

After quantitative observations of the residual imprints and the cracks induced during Berkovich nanoindentations (at 400 mN), the material toughness was obtained using the relationship 3 [9]

$$K_{Ic} = \xi \left(\frac{a}{l}\right)^{n} \left(\frac{E}{H}\right)^{m} \frac{P}{c^{\frac{3}{2}}} \tag{3}$$

in which E and H are the elastic modulus and the hardness obtained through Berkovich nanoindentations, P the peak load, a the indentation length from apex to center, l the fracture length from indentation apex, c the fracture length from indentation center, ξ a geometrical parameter depending on tip geometry assumed 1.073×0.015, n is assumed 0.5 and m is assumed 1.5 [9]. SEM images (not reported) have shown pores with approximate size ranging from few μm up to 20 μm and a decreasing interpore distance with sintering temperature. Cracks for toughness calculation were selected considering only those showing straight path not affected by defects or pores occurring on the sample surface.

2.3. Tensile strength

The tensile strength of the bulk materials was characterized through a combined experimental and theoretical approach.

Spherical indentations were performed as described in 2.1. The spherical tip pressed against the glass-ceramic surface generates cracks. All spherical residual indents were analysed by the confocal laser microscope to determine the occurence of radial or conical cracks. If radial cracks occur, an average number of radial cracks was obtained for each process temperature.

In [10], Seagraves *et al.* determined the number of radial cracks (n) upon spherical indentation on brittle material characterized by a given fracture toughness (K_{Ic}) as

$$n = \frac{2\pi a\sigma^2}{K_{Ic}^2}\left(1 + \frac{K_{Ic}}{\sigma\sqrt{2\pi a}}\sqrt{2\left(\frac{\pi a\sigma^2}{K_{Ic}^2} - 1\right)}\right) \tag{4}$$

where a is the characteristic material flaw size and σ is the tensile stress promoting the fracture.

A relationship between tensile strength and intrinsic flaw size was assessed by solving (4) for σ, introducing in (4) the values found at each temperature for K_{Ic}, from the Berkovich indentation study, and n, through laser microscopy.

2.4. Statistical Analysis

Statistical analyses were carried out on the results obtained from sections 2.1, 2.2 and 2.3: Shapiro-Wilk tests to determine data normality, Mann-Whitney U tests and Kruskal-Wallis tests to compare two and multiple data groups respectively (significance level $\alpha = 0.05$).

3. Results and Discussion

Figure 1a shows the elastic modulus (Poisson ratio assumed $\nu = 0.28$) found at different sintering temperatures for each load (Berkovich and spherical indentation results are reported for comparison purposes). The elastic modulus at $600°C$ and $650°C$ was statistically lower than the elastic modulus at $700°C$ and higher. This result is consistent with the increase of mechanical properties with crystallisation [11, 12] and supported by previous studies on bulk materials obtained with the same procedure [7], which have identified a higher crystallinity associated with higher sintering temperatures.

The values of elastic modulus obtained at 50 mN and 100 mN are considered to be representative of the material.

Values obtained from smaller loads were discarded, as the indentation depth and contact area were too small compared to surface imperfections and post-sintering residual micro- or nano-pores.
Indentations at 200 mN were discarded as confocal imaging revealed fractures, which induce underestimation of elastic properties.

The elastic moduli of samples sintered at lower temperatures, ($600°C$ and $650°C$), are comparable with the estimated bulk elastic modulus of 45S5 bioactive glass [1]; while the elastic modulus of samples sintered between $700°C$ and $850°C$ are comparable with the bulk modulus evaluated for CEL2 bioactive glass [13].

Figure 2(a) shows the crack length measuring scheme on confocal laser image of a Berkovich indentation on a $600°C$ sample; figure 2(b) shows the same residual imprint through a Scanning Electron Microscope (SEM) image.

The material toughness with respect to the sintering temperature is shown in figure 1b. Samples sintered at or below $750°C$ exhibited a fracture toughness statistically lower than samples heat-treated at $800°C$ and $850°C$. This is consistent with the increase of crystallization at higher temperature, as found in [7], yielding a subsequent increase in mechanical properties [12, 11]; the toughness values were found to be comparable to

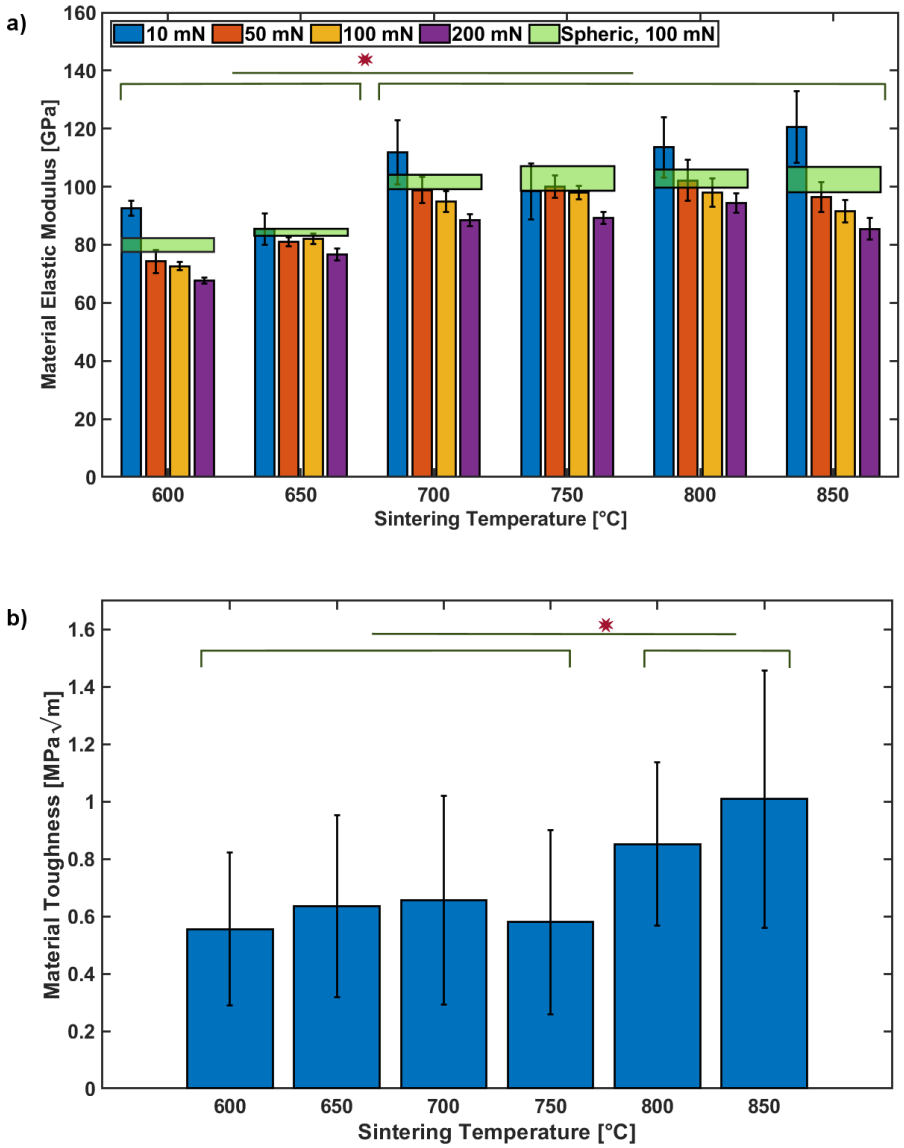

Figure 1: a) Elastic Modulus for each sintering temperature, peak load and indenter tip. Where not specified, a Berkovich tip was utilized. b) Fracture toughness for each sintering temperature, obtained as explained in 2.2.

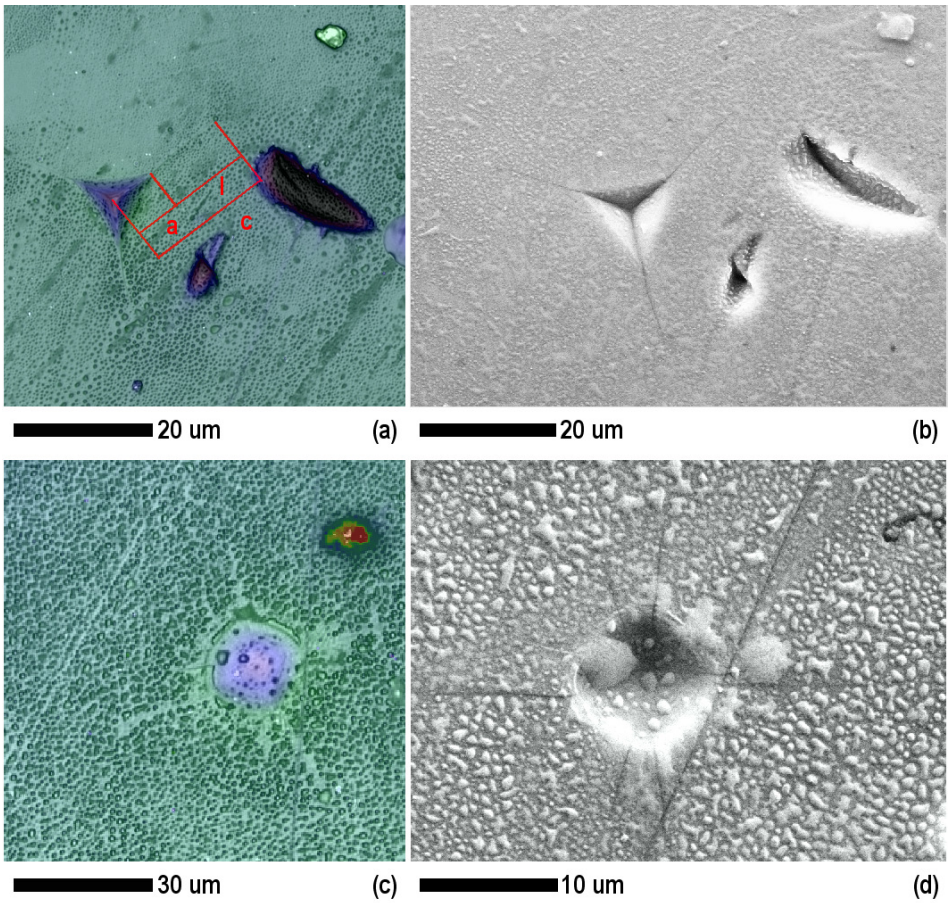

ibrahimi

Figure 2: Representative images of Berkovich (200 mN) (a,b) and Spherical (400 mN) (c,d) indentations, obtained with confocal laser (a,c) and SEM (b,d) on the sample sintered at 600 C.

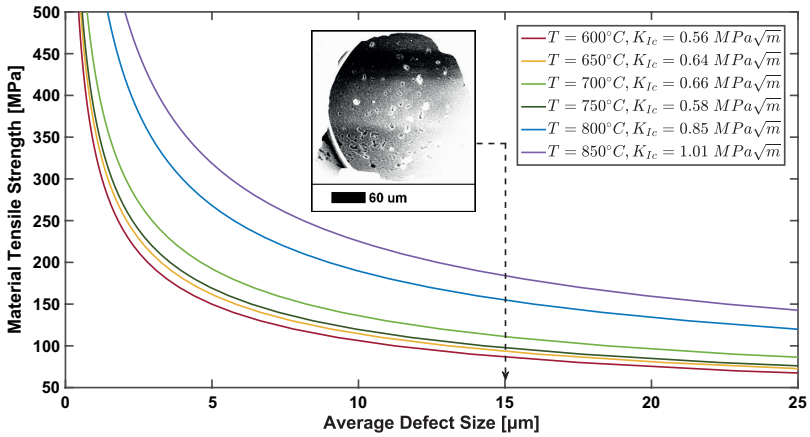

Figure 3: Tensile strength *vs average defect size and fracture toughness, obtained as explained in 2.3. Inset: SEM image of the inside of a pore, highlighting material defects at* $800°C$.

those of 45S5 glass [14]. Previous XRD analyses showed the development of combeite, tremolite and sodium calcium silicate crystalline phases in 47.5B-derived glass-ceramics sintered above $750°C$. [7]. As only straight cracks have been considered, we assumed that crystalline domains did not affect the crack length. Figure 2(c) and 2(d) show the radial cracks obtained upon spherical indentations observed through confocal microscope and SEM. The average number of cracks increases with the sintering temperature, from 3 ($600°C$) to 5 ($850°C$) owing to surface defects promoting cracks onset and propagation.

Figure 3 shows that tensile strength, as a function of flaw size, increases with the sintering temperature. At a representative defect size of 15 μm the tensile strength assessed through this method ranges between 80 MPa and 180 MPa approximately. For comparison, the bulk tensile strength of 45S5 glass is 88 MPa [14].

4. Conclusions

The mechanical characterization of 47.5B-based materials sinter-crystallzed between $600°C$ and $850°C$, was carried out. The elastic modulus increases from 80 GPa (up to $650°C$) to 100 GPa (from $700°C$); while toughness increases from 0.52 $MPa\sqrt{m}$ ($600°C$) to 1 $MPa\sqrt{m}$ ($850°C$). The increase of mechanical properties is attributable to higher crystallization occurring above $700°C$.
Tensile strength as a function of defect size was found on the basis of fracture mechanics arguments. Figure 3 is a potential tool to be used in applications once an estimated typical defect size is assessed with an independent measure.
The mechanical properties of 47.5B-derived glass-ceramics are comparabile with those of other bioactive glasses evaluated in literature, making 47.5B potentially suitable for application to bone-scaffold devices.

References

[1] A. A. El-Rashidy, J. A. Roether, L. Harhaus, U. Kneser, A. R. Boccaccini, *Acta Biomaterialia* **62**, 1 (2017).

[2] F. Shah, J. Czechowska, *Bioactive Glasses*, H. Ylänen, ed. (Woodhead Publishing, 2018), pp. 201–233, second edn.

[3] R. Bento, A. Gaddam, P. Oskoei, H. Oliveira, J. M. F. Ferreira, *Materials* **14**, 5946 (2021).

[4] M. N. Rahaman, *et al.*, *Acta Biomaterialia* **7**, 2355 (2011).

[5] F. Baino, E. Fiume, *Materials Letters* **245**, 14 (2019).

[6] E. Fiume, *et al.*, *Acta Biomaterialia* **119**, 405 (2021).

[7] E. Fiume, G. Serino, C. Bignardi, E. Vernè, F. Baino, *Applied Sciences* **10**, 8279 (2020).

[8] G. Pharr, W. Oliver, *Journal of Materials Research* **4**, 1564 (1992). An optional note.

[9] R. Dukino, M. Swain, *Journal of American Ceramics Society* pp. 299–304 (1992).

[10] A. N. Seagraves, R. A. Radovitzky, *J. Appl. Mech.* **80** (2013).

[11] F. Serbena, I. Mathias, al., *Acta Materialia* pp. 216–228 (2015).

[12] J. Daguano, K. a. Strecker, *Journal of Mechanical Behavior of Biomedical Materials* **14**, 78 (2012).

[13] M. Shahgholi, *et al.*, *Journal of the European Ceramic Society* pp. 2403–2409 (2016).

[14] Q. Fu, E. Saiz, M. N. Rahaman, A. P. Tomsia, *Advanced Functional Materials* **23**, 5461 (2013).